Date of publication xxxx 00, 0000, date of current version xxxx 00, 0000.
Digital Object Identifier 10.1109/ACCESS.2017.Doi Number

Impedance Bandwidth Improvement of a Planar Antenna Based on Metamaterial-Inspired T-Matching Network

Mohammad Alibakhshikenari[1]*, *Member, IEEE,* Bal S. Virdee[2], *Senior Member, IEEE,* Pancham Shukla[2], *Member, IEEE*, Yan Wang[3], *Member, IEEE*, Leyre Azpilicueta[4], *Senior Member, IEEE,* Mohammad Naser-Moghadasi[5], Chan H. See[6], *Senior Member, IEEE,* Issa Elfergani[7,8], *Senior Member, IEEE*, Chemseddine Zebiri[9], *Member, IEEE*, Raed Abd-Alhameed[7], *Senior Member, IEEE,* Isabelle Huynen[10], *Senior Member, IEEE,* Jonathan Rodriguez[8], *Senior Member, IEEE,* Tayeb A. Denidni[11], Fellow, *IEEE,* Francisco Falcone[12,13], *Senior Member, IEEE,* and Ernesto Limiti[1], *Senior Member, IEEE*

[1]Electronic Engineering Department, University of Rome "Tor Vergata", Via del Politecnico 1, 00133 Rome, Italy
[2]Center for Communications Technology, London Metropolitan University, London N7 8DB, U.K.
[3]Key Laboratory of Electronic Equipment Structure Design, Ministry of Education, Xidian University, Xi'an 710071, China
[4]School of Engineering and Sciences, Tecnologico de Monterrey, Monterrey NL 64849, Mexico
[5] Department of Electrical and Computer Engineering, Science and Research Branch, Islamic Azad University, Tehran 14778-93855, Iran
[6]School of Engineering and the Built Environment, Edinburgh Napier University, Edinburgh EH10 5DT, U.K.
[7]Faculty of Engineering & Informatics, University of Bradford, Bradford BD7 1DP, U.K.
[8]Instituto de Telecomunicações, Campus Universitário de Santiago, 3810-193 Aveiro, Portugal
[9]Laboratoire d'Electronique de Puissance et Commande Industrielle (LEPCI), Department of Electronics Engineering, University of Ferhat Abbas, Sétif -1-, Sétif 19000, Algeria
[10]Institute of Information and Communication Technologies, Electronics and Applied Mathematics, Université Catholique de Louvain, Belgium
[11] Institut National de la Recherche Scientifique (INRS), University of Quebec, Montréal, Québec H5A 1K6 Canada
[12]Electric, Electronic and Communication Engineering Department, Public University of Navarre, 31006 Pamplona, Spain
[13]Institute of Smart Cities, Public University of Navarre, 31006 Pamplona, Spain

* Corresponding author: Mohammad Alibakhshikenari (e-mail: alibakhshikenari@ing.uniroma2.it)

ABSTRACT In this paper a metamaterial-inspired T-matching network is directly imbedded inside the feedline of a microstrip antenna to realize optimum power transfer between the front-end of an RF wireless transceiver and the antenna. The proposed T-matching network, which is composed of an arrangement of series capacitor, shunt inductor, series capacitor, exhibits left-handed metamaterial characteristics. The matching network is first theoretically modelled to gain insight of its limitations. It was then implemented directly in the 50-Ω feedline to a standard circular patch antenna, which is an unconventional methodology. The antenna's performance was verified through measurements. With the proposed technique there is 2.7 dBi improvement in the antenna's radiation gain and 12% increase in the efficiency at the center frequency, and this is achieved over a significantly wider frequency range by a factor of approximately twenty. Moreover, there is good correlation between the theoretical model, method of moments simulation, and the measurement results.

INDEX TERMS *T*-matching circuit, microstrip antenna, metamaterial, transmission-line, impedance matching.

I. INTRODUCTION

Microstrip antennas have become popular for use in many wireless systems due to their planar profile, ease of fabrication and low manufacturing cost. Moreover, such antennas allow ease of integration with RF circuit components [1]. As a result, the use of planar based antenna configurations enables the integration of communication capabilities in a wide range of applications in the context of Industry 4.0 technologies such as Internet of Things (IoT) or vehicular communications, among others. This has been made possible by the design of flexible and compact transceivers especially in the sub-6 GHz band for wireless sensor networks (WSN), wireless local area networks (WLAN), public land mobile networks (PLMN) and 5G communication systems. The vast number of applications which make use of wireless communication systems is leading to the need of employing different wireless systems in a cooperative way (i.e., Heterogeneous Network operation), as well as the increase in the allocated channel bandwidth. Optimal performance of these wireless systems is given, among other factors, by adequate transceiver system operation. In relation with antenna sub-systems, impedance matching is one of the main factors to consider in order to reduce reflection-coefficient and hence, increase overall coverage range and minimize overall energy consumption [2-7].

The input impedance of an antenna is typically different from the impedance of the system to which it is connected, requiring impedance matching stages in order to minimize losses. In many cases, it is possible to realize impedance matching by modifying the antenna geometry [8]. However, the main limitation of conventional microstrip antennas is their narrow impedance bandwidth (typically less than 3% for reflection-coefficient better than -10 dB). In addition, electrically thin edge-fed microstrip patch antennas usually suffer from high resonant input impedance, typically in a range of 300–500 Ω, which is challenging to directly match with a 50-Ω microstrip feedline. To maximize power transfer to and from the antenna, and therefore enhance its radiation efficiency different matching approaches have been investigated previously [9-11].

In many wireless applications the matching circuit is not always designed for optimum power transfer between the antenna and transceiver, but consideration is given to maximizing the power handling capability, reducing non-linear distortion and impedance bandwidth. In [12] the matching and impedance bandwidth enhancement is achieved by stacking the radiation patch with a parasitic element. With this technique bandwidth extension of ~19% is possible. In [13], the feeding scheme employed provides an impedance bandwidth of ~28% however the design of the feeding scheme is complex to implement in practice, which has an impact in fabrication cost. In [14], a capacitively coupled probe is used to excite a nonradiative mode close to the antenna's dominant radiation mode to realize a bandwidth of ~28%. In [15] multiple resonant modes are simultaneously excited to extend the bandwidth of a patch antenna by about 32%, however this technique is shown to adversely affect the antenna's broadside radiation pattern. In [16] the bandwidth is improved by 15.2% by exciting dual modes.

In this paper a simple and effective metamaterial-inspired wideband matching technique is proposed to enhance the radiation gain and efficiency performance of a planar antenna. The proposed matching technique uses a *T*-matching network consisting of series capacitor, shunt inductor, series capacitor configuration to realize metamaterial characteristics. The matching network is directly embedded inside the feedline of the antenna, which is an unconventional methodology. The technique is first theoretically characterized to gain an understanding of its effectiveness and is then validated through practical design and measurement.

II. IMPEDANCE MATCHED ANTENNA

The three types of lumped element matching networks that are commonly used are based on the *L*-network, π-network, and *T*-network. The advantage of *L*-network is that it only has two reactive components whose values can be tuned easily for a given load impedance. However, its impedance matching capability is limited. On the other hand, the π- or *T*-networks have the capability of providing superior impedance matching flexibility than the *L*-network because they have three reactive components that can be tuned.

Fig.1 shows equivalent circuit of a typical *L*- and *T*-matching network. The reactive components can be either lumped elements or realized using transmission-lines based on microstrip integrated circuit technology. Capacitors can be realized using interdigital or low impedance microstrip-lines and inductors can be realized using high impedance microstrip-lines. Reactive components realized using microstrip-lines can however result in a larger circuit size.

The reactive components in the network control the reflection-coefficient between the antenna and matching network. In practice the capacitance values are adjusted or tuned until the reflection-coefficient of the antenna is lower than a specified threshold value, which is typically -10 dB, to (i) reduce system complexity, (ii) maintain the matching performance, and (iii) maximize RF power to the antenna.

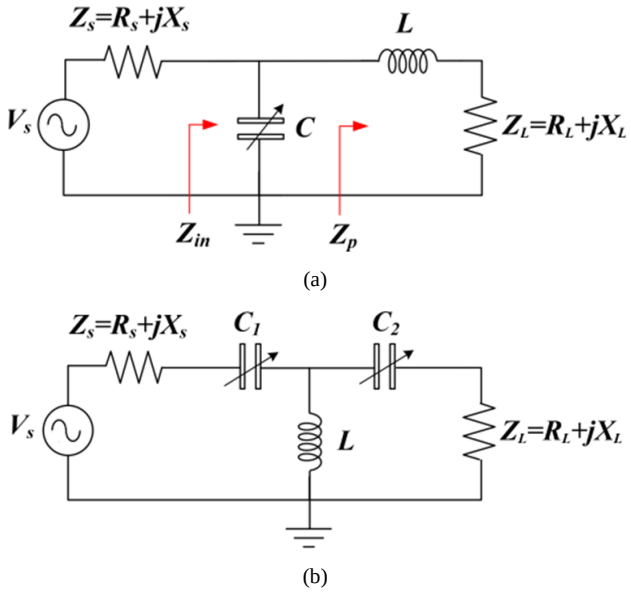

Fig.1. (a) Equivalent circuit of *L*-matching network, and (b) equivalent circuit of *T*-matching network.

To determine the effect of *LC* reactive components on the input impedance Z_{in} of the *L*-network in Fig.1(a) the network is first represented in a simplified form in Fig.2, where the impedance Z_q accounts for inductance *L* and the load impedance $Z_L = R_L + jX_L$.

$$Z_{in} = \frac{\frac{1}{\omega C}(B-jA)}{A+j\left(B-\frac{1}{\omega C}\right)} = R + jX \qquad (1)$$

Where the real and imaginary impedances are:

$$R = A/[(\omega AC)^2 + (\omega BC - 1)^2] \qquad (2)$$

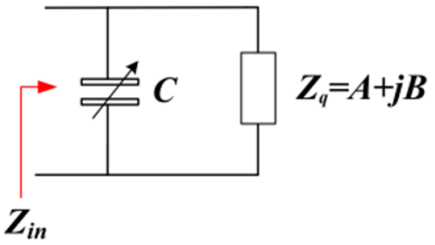

Fig.2. Impedance Z_{in} of the *L*-matching network in Fig.1.

$$X = [B - \omega C(A^2 + B^2)]/[(\omega AC)^2 + (\omega BC - 1)^2] \quad (3)$$

By dividing Eqn.(2) by (3) it can be shown that

$$\omega C = (BR - AX)/R(A^2 + B^2) \quad (4)$$

Substituting Eqn. (4) into (2) and (3), it can be shown that

$$[R - (A^2 + B^2)/2A]^2 + X^2 = [(A^2 + B^2)/2A]^2 \quad (5)$$

Where $A = R_L$ and $B = \omega L + X_L$

Eqn.(5) describes a circle whose center and radius, i.e. the impedance position, is a function of the inductive and capacitive reactance and the load impedance. This equation reveals that the center and radius of the impedance circle can be changed by tweaking either one or both inductance and capacitance in the circuit to effect matching. Unlike the *L*-network a *T*-network can provide superior impedance matching because it has three reactive components that can be tuned. In the next section a *T*-matching circuit is explored in the reduction of mismatch between the antenna and RF front-end circuit.

III. *T*-COMPENSATION CIRCUIT

In a real-world scenario, the matching network is connected to the antenna using a transmission-line. The proposed *T*-matching network in Fig.3 comprises an arrangement of series capacitor, shunt inductor, series capacitor. Assuming $C_1 = C_2 = C/2$ it can be shown that the propagation β, the phase velocity v_p, and group velocity v_g are given by [17]

$$\beta = -\frac{1}{\omega\sqrt{LC}} < 0 \quad (6)$$

$$v_p = \frac{\omega}{\beta} = -\omega^2\sqrt{LC} < 0 \quad (7)$$

$$v_g = \left(\frac{\partial\beta}{\partial\omega}\right)^{-1} = +\omega^2\sqrt{LC} > 0 \quad (8)$$

Eqn. (7) and (8) show that phase and group velocities are antiparallel, which is characteristic of left-handed metamaterial [17].

The impedance Z_x seen by the signal from the transmitter is a combination of the impedance Z_1 of the transmission-line of length l and the impedance of the antenna load Z_L. Hence, to optimize power transfer between the transmitter to the antenna, we need to conjugately impedance match the impedance Z_{in} looking into the matching circuit to Z_x.

The impedance Z_x looking into the antenna load of impedance Z_L via the transmission-line of length l of impedance Z_1 is given by

$$Z_x = Z_1\left[\frac{Z_L + jZ_1 tan\beta l}{Z_1 + jZ_L tan\beta l}\right] \quad (9)$$

Then $$Z_y = \frac{\frac{L}{C_2} + j\omega L Z_x}{Z_x + j\left(\frac{\omega^2 LC_2 - 1}{\omega C_2}\right)} \quad (10)$$

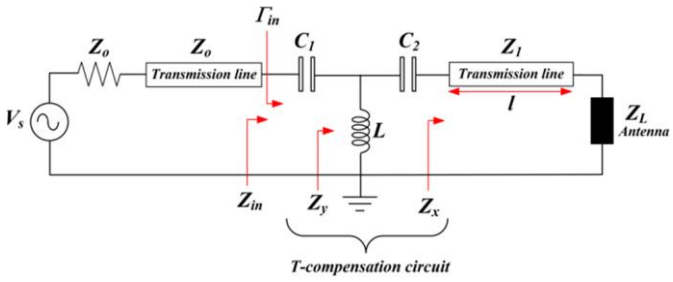

Fig.3. Equivalent circuit model of the *T*-matching network inserted between the source and the antenna.

The input impedance Z_{in} of the *T*-compensation circuit, shown in Fig.3, can be represented as $Z_{in} = R_{in} + jX_{in}$, where R_{in} and X_{in} can be determined to be given by

$$R_{in} = \frac{\frac{xL}{t}\left(\frac{1}{C_2} - \frac{\omega y}{t}\right) + \frac{\omega xL}{t}\left[\frac{y}{t} + \left(\frac{\omega^2 LC_2 - 1}{\omega C_2}\right)\right]}{\left(\frac{x}{t}\right)^2 + \left[\frac{y}{t} + \left(\frac{\omega^2 LC_2 - 1}{\omega C_2}\right)\right]^2} \quad (11)$$

$$X_{in} = \frac{\omega L\left(\frac{x}{t}\right)^2 - L\left(\frac{1}{C_2} - \frac{\omega y}{t}\right)\left[\frac{y}{t} + \left(\frac{\omega^2 LC_2 - 1}{\omega C_2}\right)\right]}{\left(\frac{x}{t}\right)^2 + \left[\frac{y}{t} + \left(\frac{\omega^2 LC_2 - 1}{\omega C_2}\right)\right]^2} - \omega C_1 \quad (12)$$

Where

$$x = Z_L Z_1(1 + tan^2\beta l)$$

$$y = tan^2\beta l(Z_1^2 - Z_L^2)$$

$$t = Z_1^2 + Z_L^2 tan^2\beta l$$

Reflection-coefficient (Γ_{in}) at the input port of the antenna is a measure of how much RF power is reflected from the antenna. This parameter therefore determines how much RF power is radiated by the antenna. It also has an impact on the radiation efficiency of the antenna which is calculated in terms

of the ratio of the radiated power to the power delivered to the load. The reflection-coefficient looking at the antenna via the *T*-compensation circuit is given by:

$$\Gamma_{in} = \frac{R_{in}^2+X_{in}^2-Z_o^2-jR_{in}}{(R_{in}+Z_o)^2+X_{in}^2} \qquad (13)$$

where R_{in} and X_{in} are defined by Eqns. (11) and (12). Eqn.(13) indicates that the center frequency and bandwidth of the matching system can be controlled by simply using appropriate values of the capacitances C_1 and C_2 and inductance L. For a *T*-matching circuit the relationship between bandwidth and reflection-coefficient is derived in [18] to be given by

$$BW \approx \frac{\sqrt{|\Gamma_{in}|}}{1-|\Gamma_{in}|} \qquad (14)$$

Eqn.(14) indicates that by appropriately selecting R_{in} and X_{in} the bandwidth of the matching network can be optimized.

The basic *T*-match circuit, shown in Fig.4, allows to set impedance transformation ratio and Q-factor/matching bandwidth of circuit independently.

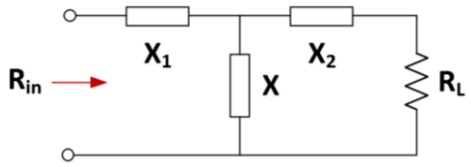

Fig.4. *T*-matching circuit.

$$Q_1 = \frac{X_1}{R_{in}} \qquad Q_2 = \frac{X_2}{R_L} \qquad (15)$$

The *T*-matching circuit can be decomposed to two *L*-match circuits, as shown in Fig.5. By series-to-parallel transformation as shown in From Fig.6 [19][20],

$$Q_1 = \frac{R_I}{X_A} \qquad Q_2 = \frac{R_I}{X_B} \qquad (16)$$

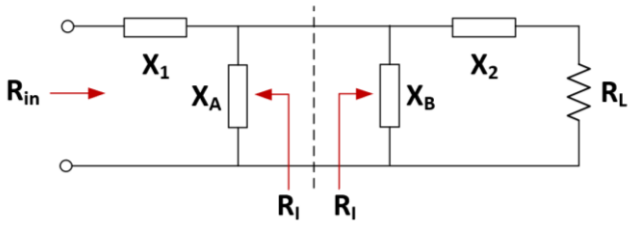

Fig.5. *T*-matching circuit decomposed to two *L*-match circuits.

$$R_{in,p} = R_I = R_{in}(1+Q_1^2) \quad R_{L,p} = R_I = R_L\left(1+\frac{1}{Q_2^2}\right) \qquad (17)$$

$$X_{1,p} = X_I\left(1+\frac{1}{Q_1^2}\right) \qquad X_{2,p} = X_I\left(1+\frac{1}{Q_2^2}\right) \qquad (18)$$

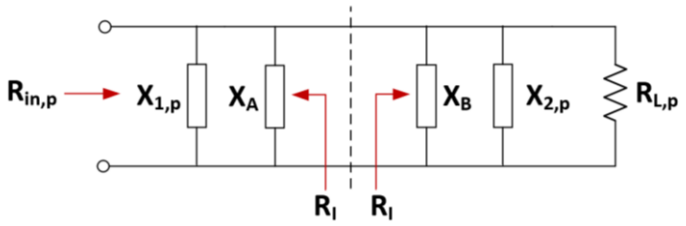

Fig.6. *T*-matching after series to parallel transformation.

Rearranging Eqn.(17)

$$Q_1 = \sqrt{\frac{R_I}{R_{in}}-1} \qquad Q_2 = \sqrt{\frac{R_I}{R_L}-1} \qquad (19)$$

The total Q of the circuit is given by

$$Q = Q_1 + Q_2 = \sqrt{\frac{R_I}{R_{in}}-1} + \sqrt{\frac{R_I}{R_L}-1} \qquad (20)$$

At resonant frequency, $|X_A| = |X_{1,p}|$ and $|X_B| = |X_{2,p}|$.

Therefore, $X_A = X_1\left(1+\frac{1}{Q_1^2}\right)$ $X_B = X_2\left(1+\frac{1}{Q_2^2}\right)$

The above relationships allow the design of the preliminary *T*-matching circuit. The design procedure involves: (i) finding R_I using Eqn.(20) from given R_L, R_{in} and Q; (ii) calculating Q_1 and Q_2 using Eqn.(19); (iii) finding X_1 and X_2 using Eqn.(15), and (iv) finding X_A and X_B using Eqn.(16).

The expression for the gain of the circular patch antenna can be determined using [21]

$$G = \eta D \qquad (21)$$

Where the efficiency η is given by

$$\eta = \frac{P_r}{P_T} \qquad (22)$$

Where P_r is the radiated power into space, and P_T is the total power delivered to the antenna. This expression indicates that the efficiency of the antenna is independent of frequency. The directivity of the antenna *D* is given by [22]

$$D = \frac{\frac{1}{2}Re\left(E_\theta H_\emptyset^* - E_\emptyset H_\theta^*\right)|_{\theta=0}}{P_r/4\pi r^2} \qquad (23)$$

Taking Eqn.(23) and (22), Eqn.(21) can be written as

$$G_e = \frac{4\pi r^2}{P_T}.\frac{1}{2}Re\left(E_\theta H_\emptyset^* - E_\emptyset H_\theta^*\right)|_{\theta=0}$$
$$= \frac{4\pi r^2}{P_T}.\frac{1}{2\eta_o}\left(|E_\theta|^2 + |E_\emptyset|^2\right)|_{\theta=0} \qquad (24)$$

Where $\eta_o = 120\pi\Omega$, the free-space impedance.

The far-field electric field components are given by [22]

$$E_\theta = j^n \frac{Vak_o}{2r}.\frac{e^{-jk_o r}}{r}\cos n\emptyset \times [J_{n+1}(k_o a\, sin\theta) - J_{n-1}(k_o a\, sin\theta)] \quad (25)$$

$$E_\phi = j^n \frac{Vak_o}{2r}.\frac{e^{-jk_o r}}{r}\cos\theta \sin n\emptyset \times [J_{n+1}(k_o a\, sin\theta) - J_{n-1}(k_o a\, sin\theta)] \quad (26)$$

Where $V = hE_oJ_n(k_oa)$, h is the thickness of the substrate, a is effective radius of the circular patch, $J_n(ka)$ is the Bessel function of order n and $k_o = \omega/c$.

From Eqn.(25) and (26), for n = 1, we obtain

$$(|E_\theta|^2 + |E_\emptyset|^2)|_{\theta=0} = \left(\frac{Vak_o}{2r}\right)^2 \quad (27)$$

The expression for effective gain given by Eqn.(24) then becomes

$$G = \frac{\pi}{2\eta_o}(Vak_o)^2.\frac{1}{P_T} \quad (28)$$

The resonant resistance *R* can be calculated using

$$R = \frac{V^2}{2P_T} \quad (29)$$

Then from Eqs. (28) and (29),

$$G = \frac{\pi R}{\eta_o}\left(\frac{2\pi a f_r}{c}\right)^2 \quad (30)$$

Where f_r is the resonant frequency of the dominant mode (TM_{11}). Eqn.(30) indicates the gain of the circular patch antenna is affected by the power delivered to it.

Assuming $C_1 = C_2 = C/2$ in Fig.3, the ABCD matrix of the *T*-matching network is given by [23]

$$\begin{bmatrix}\bar{A} & \bar{B}\\ \bar{C} & \bar{D}\end{bmatrix} = \begin{bmatrix}1 & \bar{X}_c\\ 0 & 1\end{bmatrix}\begin{bmatrix}1 & 0\\ \bar{Y}_L & 1\end{bmatrix}\begin{bmatrix}1 & \bar{X}_c\\ 0 & 1\end{bmatrix} \quad (31)$$

This matrix can be simplified to

$$\begin{bmatrix}\bar{A} & \bar{B}\\ \bar{C} & \bar{D}\end{bmatrix} = \begin{bmatrix}1+\bar{X}_c\bar{Y}_L & \bar{X}_c(1+\bar{X}_c\bar{Y}_L)+\bar{X}_c\\ \bar{Y}_L & 1+\bar{X}_c\bar{Y}_L\end{bmatrix} \quad (32)$$

Where $\bar{X}_c = -j2/\omega C Z_o$ and $\bar{Y}_L = -jZ_o/\omega L$.

The insertion loss is defined as [23]

$$IL = 10log\frac{P_{Lb}}{P_{La}} \quad (33)$$

Where P_{Lb} is power delivered to the load before inserting the *T*-matching network, and P_{La} is power delivered to the load after inserting the network. For the two-port *T*-matching network in Fig.3 that is symmetrical and reciprocal, the following conditions apply [23]

1. $\bar{A} = \bar{D}$ 2. $\bar{A}\,\bar{D} - \bar{B}\bar{C} = 0$
3. $\bar{A}$ & $\bar{D}$ are real 4. $\bar{B} = \bar{C}$ are imaginary

Hence the insertion loss in terms of ABCD matrix is given by [23]

$$IL = 10log\left[1 + \left(\frac{\bar{B}}{2j} - \frac{\bar{C}}{2j}\right)^2\right] \quad (34)$$

Therefore, the insertion loss introduced by inserting the two-port *T*-matching network can be shown to be given by

$$IL = 10log\left[1 + \left[\frac{2}{\omega C}\left(\frac{1}{\omega^2 LC} - \frac{1}{Z_o}\right) + \frac{Z_o}{2\omega L}\right]^2\right] \quad (35)$$

The gain of the *T*-matching network in Eqn.(30) is therefore affected by the insertion loss which is defined in Eqn.(35)

In the next section it is shown that with proper selection of C_1, C_2, and L a high gain and high radiation efficiency can be obtained over a wide frequency band. However, this does introduce some complexity in the design as each variable capacitor needs to be controlled separately. Nevertheless, the proposed technique is amenable to electronic tuning hence allowing controllable matching capability according to system requirements.

IV. DESIGN EXAMPLE USING METAMATERIAL INSPIRED *T*-MATCHING NETWORK

A standard circular microstrip antenna was designed at 4 GHz using FR-4 lossy substrate with a relative permittivity of 4.3, thickness of 1.6 mm, and tanδ of 0.025. The radius of the circular patch is 11.2 mm. The patch antenna is excited using a microstrip feedline. Fig.7(a) shows the equivalent circuit model of the distributed transmission-line feed and the patch antenna. The *LC* component values of the feedline were chosen such that its lowpass filter response was well above the resonant frequency of the antenna so that it had no impact on the antenna's performance. The reflection-coefficient of the antenna predicted by theory and simulation in Fig.8 show it resonates at 4 GHz with a high-Q and hence has a narrow impedance bandwidth. The measured results show a bandwidth of 0.1 GHz for S_{11}≤-10 dB with an optimum reflection-coefficient value of -12 dB at 4 GHz.

Microstrip feedline length determines the input impedance of the antenna. Hence, a *T*-matching circuit is directly embedded in the feedline, which is an unconventional technique. The matching circuit used here is a metamaterial structure that exhibits left-handed properties of negative refractive index when interacts with electromagnetic signals [17]. The metamaterial characteristics are realized here with a *T*-network composed of series capacitance, shunt inductance, and series capacitance circuit, as per schematic diagram in Fig.7(b). The dispersion diagram of the antenna with the matching circuit in Fig.9 show the phase variation is virtually zero at 4 GHz. The dispersion diagram was computed using CST Microwave Studio which is 3D electromagnetic simulation tool. The antenna structure was modelled in CST and its boundary conditions, which defines the radiating environment of the model, were set appropriately so that the simulator effectively saw open space around the antenna. The

Eigenmode Solver in CST was used to obtain the dispersion diagram as described in [24].

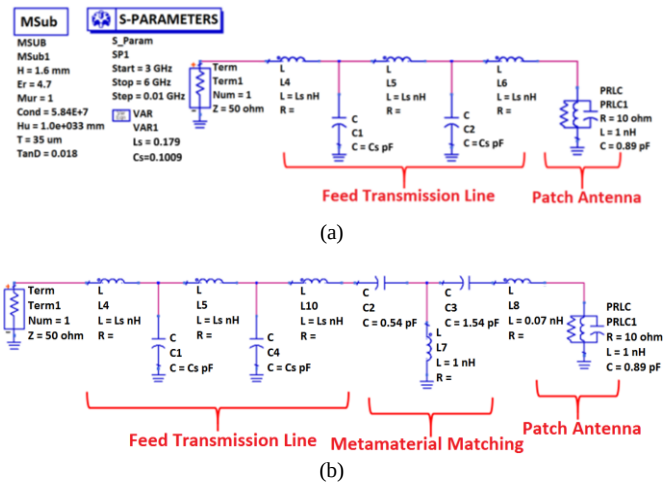

Fig.7. (a) Equivalent circuit model of feedline and patch antenna, and (b) circular patch antenna loaded with metamaterial matching network using Keysight Technologies' Advance Design System (ADS).

The reflection-coefficient response in Fig.8 by theory, simulation, and measurement show that with the inclusion of the metamaterial matching network the antenna's impedance bandwidth is significantly improved. It is evident from Fig.8 that magnitude of reactive components constituting the *T*-matching circuit have a great influence on the Q-factor of the antenna. The results of the parametric study in Fig.10 show how the parameters constituting the *T*-matching circuit effect the reflection-coefficient response. The optimum values are: C_1 = 0.5462 pF, C_2 = 1.545 pF and L = 1.1586 nH. The fabricated antenna with the matching network is shown in Fig.11. Its measured reflection-coefficient in Fig.8 is better than -18 dB at 4 GHz. The magnitude of the geometrical parameters corresponding to the lumped element values, which are annotated in Fig.11, are given in Table I.

Table I. Antenna's geometrical parameters

Parameters	Size (mm)
L	54
W	29
R	11.2
L_f	28
W_f	2.47
L_s	2.3
W_s	0.5
Radius of shunt via-hole	0.5
Thickness of FR-4 substrate	1.6

Simulated current distribution without and with the *T*-matching circuit at 4 GHz is shown in Fig.12. The size and color of the arrow indicate the magnitude and intensity of the current. The rainbow-colored band defines the magnitude of the intensity associated with the color of the arrows. It is evident that the current distribution over the antenna with the *T*-matching circuit results in current concentration at the shorting pin of the matching circuit in the feedline. Despite this the magnitude of the current intensity associated with the colored arrows over the two antennas, i.e., without and with the matching network, as specified in the colored bands show the current intensity is comparable. The E-field distribution over the antenna without and with the *T*-matching circuit is shown in Fig.13. It is observed from this figure that the E-field intensity is strongest at the top and bottom portions of the patch however the E-field intensity is unaffected with the inclusion of the *T*-matching circuit.

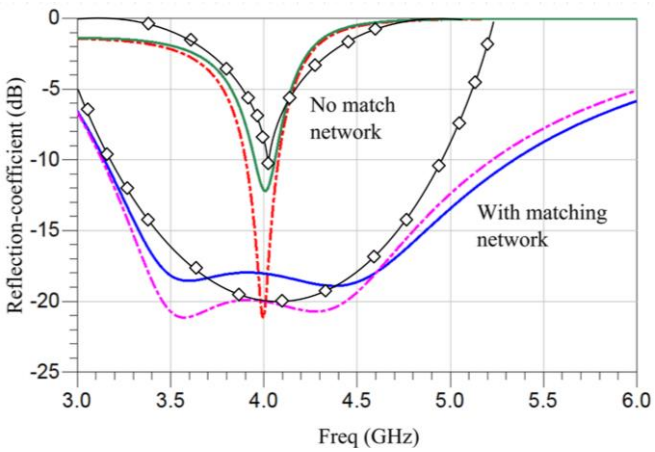

Fig.8. Theoretical, simulated and measured reflection-coefficient response of the antenna without and with the metamaterial-inspired matching network. Black diamond studded line is prediction by theory, dotted lines indicate the simulated result, and solid lines represent the measured result.

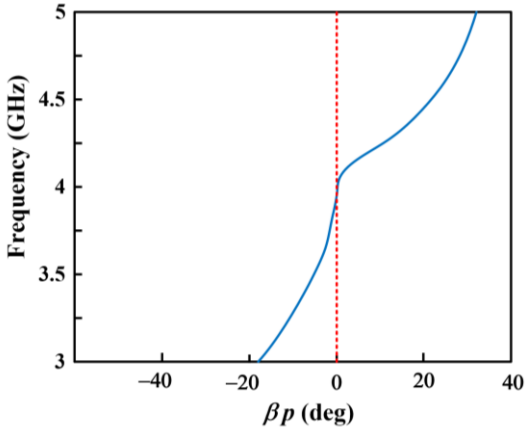

Fig.9. Dispersion diagram of the CRLH-TL feedline antenna.

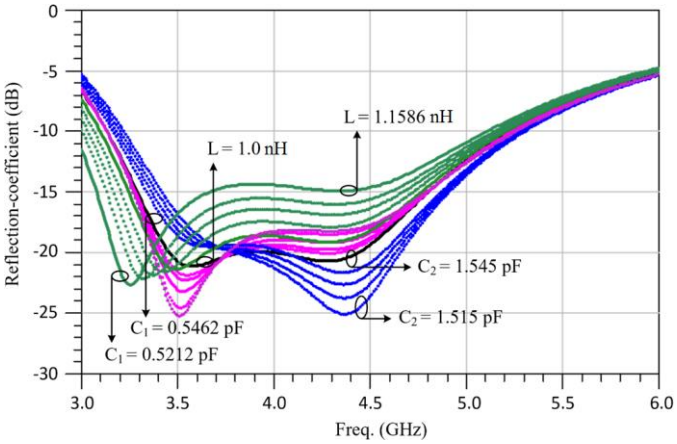

Fig.10. Effect on the reflection-coefficient response by the *T*-matching network parameters.

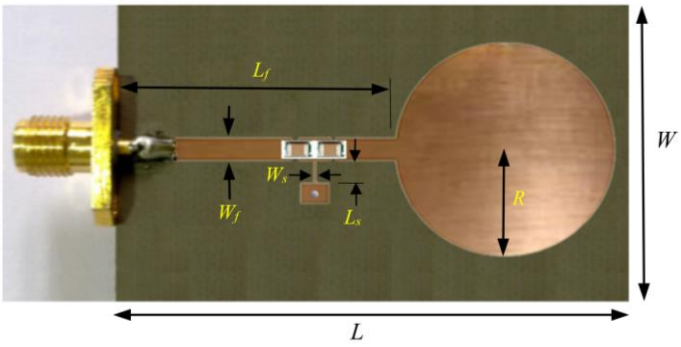

Fig.11. Photograph of the microstrip antenna incorporating the *T*-matching circuit.

The measured radiation gain and efficiency performance without and with the *T*-matching circuit are shown in Fig.14. It is evident from these results that there is substantial improvement in the radiation gain and efficiency by employing the *T*-matching circuit. This is because most of the RF power is delivered to the antenna from the source. Measured results show without the matching circuit the antenna has a peak gain and efficiency of 5.5 dBi and 59.8%, respectively, at 4 GHz. However, with the matching circuit the peak gain and peak efficiency are 8.2 dBi and 71.8%, respectively. Moreover, the gain and efficiency extend over a significantly larger bandwidth. The gain ≥6 dBi extend from 3.35-5.25 GHz, and the efficiency ≥60% extend from 3.25-5.1GHz.

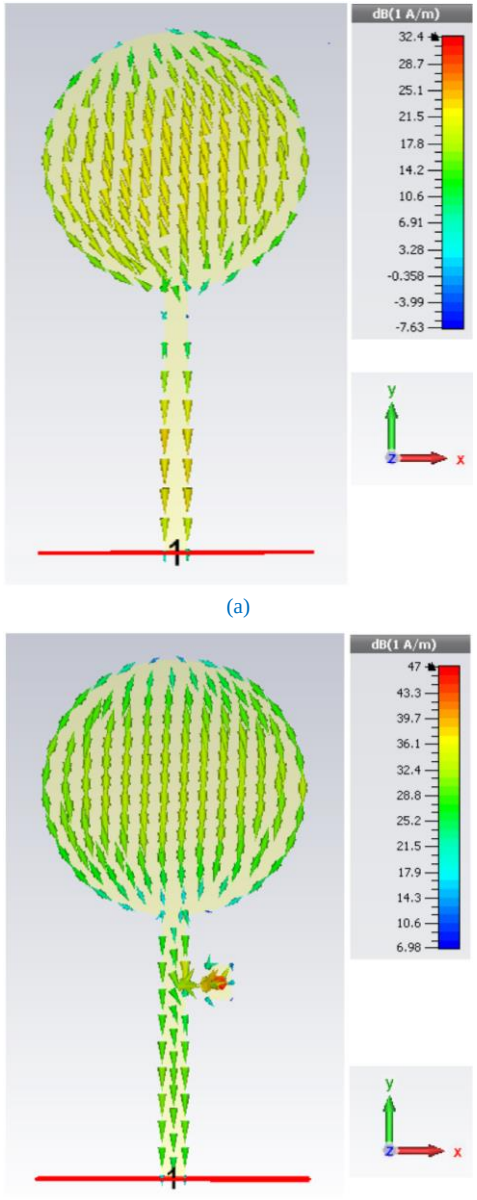

Fig.12. Surface current distribution over the antenna at 4 GHz, (a) without the *T*-matching circuit, and (b) with the *T*-matching circuit.

The radiation pattern in the E- and H-planes and the cross-polarization without and with the *T*-matching network at 4 GHz are shown in Fig. 15. The change in the radiation pattern with the *T*-matching network is marginal and, in both cases, the cross-polarization is less than -30 dB.

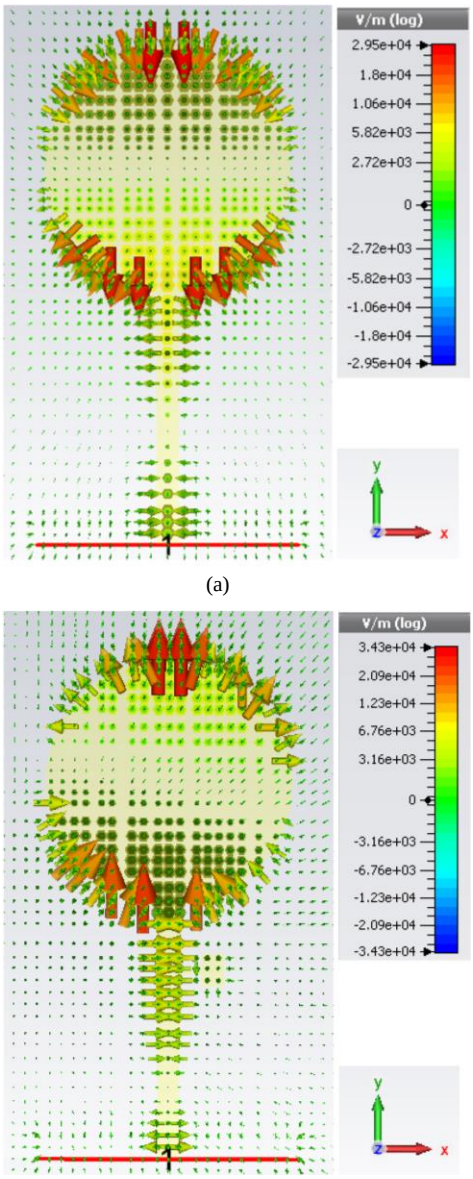

Fig.13. E-field distribution over the antenna at 4 GHz, (a) without the *T*-matching circuit, and (b) with the *T*-matching circuit.

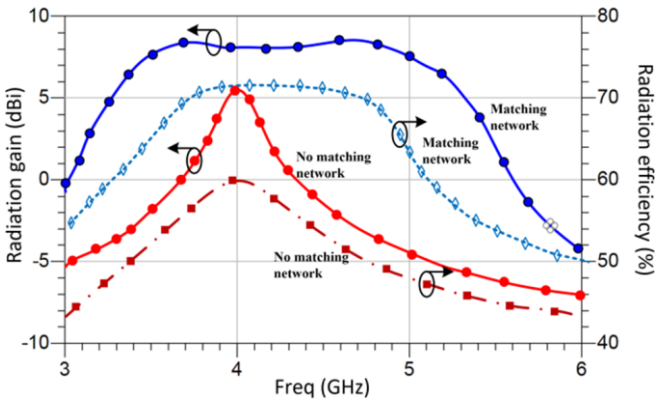

Fig.14. Measured radiation gain and efficiency response with and without the embedded *T*-matching circuit.

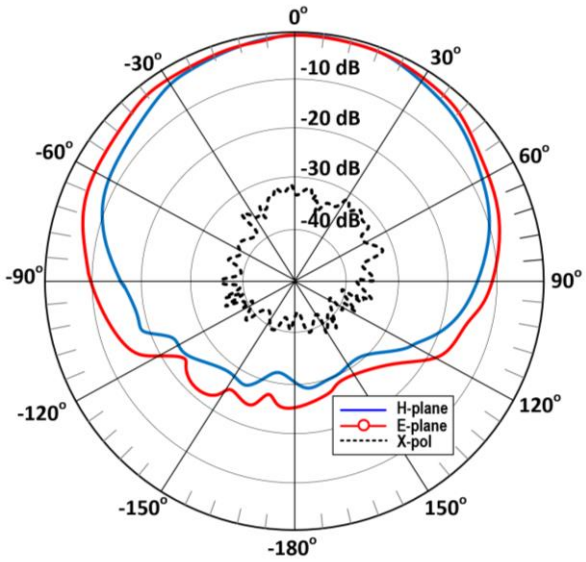

(a) With no *T*-matching circuit.

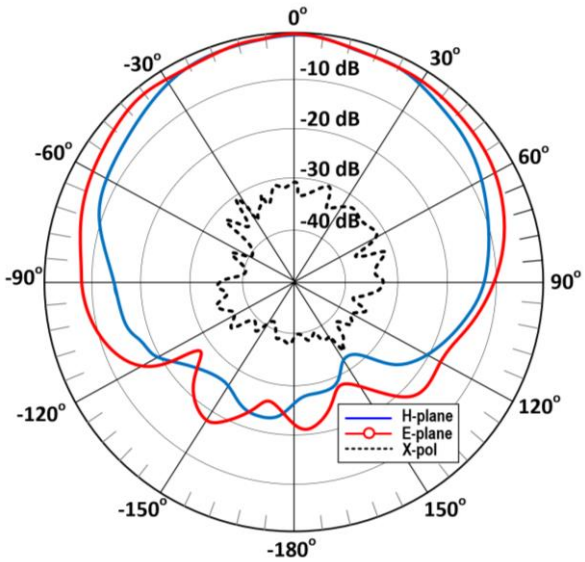

(b) With *T*-matching circuit.

Fig.15. The normalized measured radiation pattern in the E-plane and H-plane at 4 GHz, (a) without no matching circuit, and (b) with the embedded *T*-matching circuit.

Table II compares the present technique with some recently reported antenna bandwidth enhancement techniques. Impedance bandwidth enhancement of a microstrip patch antenna in [25] and [26] is achieved by loading the antenna with shorting pins and slots. In [27] the bandwidth is enhanced by simply curving the patch antenna in a partial cylindrical shape. In [28] one-dimensional electromagnetic bandgap ground structures and two-stage beam directors are employed in an inverted-L antenna topology to enhance the bandwidth. Even though the radiation efficiency of the proposed antenna is relatively low compared with the other techniques it is evident from the table that the proposed technique has a comparable gain and exhibits a substantially larger impedance

bandwidth. Moreover, its size is relatively small with the exception of [28].

Table II. Comparison of the proposed matching technique of recently reported techniques.

Ref.	Technology	Antenna size	Fractional bandwidth (%)	Peak Gain (dBi)	Peak Eff. (%)
25	Shorting pins & slots	$1.14\lambda_o \times 1.27\lambda_o \times 0.009\lambda_o$	10	11.8	94
26	Shorting pins & slots	$1.02\lambda_o \times 1.47\lambda_o \times 0.045\lambda_o$	8.8 & 4.9	6 & 8	93 & 95
27	Microstrip	$0.58\lambda_o \times 0.58\lambda_o \times 0.016\lambda_o$	9	6.28	83.5
28	One-dimensional EM bandgap ground structures & two-stage beam directors	$0.21\lambda_o \times 0.32\lambda_o \times 0.009\lambda_o$	32.5	7	95
12	Differential microstrip	$0.8\lambda_o \times 0.8\lambda_o \times 0.013\lambda_o$	18.7	8.5	80
13	Magneto-electric dipole	$0.97\lambda_o \times 0.97\lambda_o \times 0.17\lambda_o$	28.2	9.0	-
15	Shorting pin & slot	$1.17\lambda_o \times 1.17\lambda_o \times 0.055\lambda_o$	32.2	6.5	93
16	Aperture-fed with shorting pins	$1.63\lambda_o \times 0.82\lambda_o \times 0.017\lambda_o$	15.2	6.8	-
This work	Metamaterial feedline	$0.67\lambda_o \times 0.38\lambda_o \times 0.021\lambda_o$	52.5	8.2	71.8

VI. CONCLUSION

Impedance bandwidth of an antenna is determined by the matching conditions between the RF transceiver front-end and the antenna. We have demonstrated the effectiveness of employing an embedded metamaterial-based *T*-matching circuit directly implemented inside the feedline to enhance the antenna's impedance bandwidth. The measured results confirm significant improvement in the antenna's impedance bandwidth over its operating frequency range. Moreover, with the proposed technique improvement was observed in the radiation gain and efficiency too.

ACKNOWLEDGMENTS

This work is partially supported by RTI2018-095499-B-C31, Funded by Ministerio de Ciencia, Innovación y Universidades, Gobierno de España (MCIU/AEI/FEDER,UE), and British Council (UK-China-BRI Countries Education Partnership Initiative 2019), and innovation programme under grant agreement H2020-MSCA-ITN-2016 SECRET-722424, and UK Engineering and Physical Sciences Research Council (EPSRC) under grant EP/E022936/1.

REFERENCES

[1] D. M. Pozar and D. H. Schaubert, *Microstrip Antennas: The Analysis and Design of Microstrip Antennas and Arrays*, Wiley-IEEE Press, 1995.
[2] N. Engheta, "An idea for thin subwavelength cavity resonators using metamaterials with negative permittivity and permeability," IEEE Antennas Wireless Propagat. Lett., vol. 1, pp. 10–13, January 2002.
[3] M. A. Antoniades and G. V. Eleftheriades, "Compact, linear, lead/lag metamaterial phase shifters for broadband applications," IEEE Antennas Wireless Propag. Lett., Vol. 2, No. 1, pp. 103–106, July 2003.
[4] H. Okabe, C. Caloz, and T. Itoh, "A compact enhanced-bandwidth hybrid ring using an artificial lumped-element left-handed transmission- line section," IEEE Trans Microwave Theory Tech., vol. 52, no. 3, pp. 798-804, March 2004.
[5] I. S. Nefedov, and S. A. Tretyakov, "On potential applications of metamaterials for the design of broadband phase shifters," Microwave Optical Technol. Lett., vol. 45, no. 2, pp. 98–102, April 2005.
[6] M. A. Antoniades and G. V. Eleftheriades, "A broadband series power divider using zero-degree metamaterial phase-shifting lines," IEEE Microwave Wireless Comp. Lett., Vol. 15, No. 11, pp. 808–810, Nov. 2005.
[7] D. R. Jackson and A. A. Oliner, "Leaky-Wave Antennas," in Modern Antenna Handbook, C. A. Balanis, Ed. New York: John Wiley & Sons, 2008.
[8] J. C. e. Silva, D. F. Mamedes, T. d. S. Evangelista and T. R. de Sousa, "Parametric analysis of angular inset-feed in circular microstrip patch antenna," 2015 SBMO/IEEE MTT-S International Microwave and Optoelectronics Conference, Porto de Galinhas, 2015, pp. 1-5.
[9] S. E. Sussman-Fort and R. M. Rudish, "Non-Foster impedance matching of electrically-small antennas," IEEE Trans. Antennas Propag. vol. 57, 2009, 2230-2241.
[10] A. H. Dorrah, M. Chen, and G. V. Eleftheriades, "Bianisotropic Huygens' metasurface for wideband impedance matching between two dielectric media," IEEE Trans. Antennas Propag., vol. 66, no. 9, Sep. 2018, pp. 4729–4742.
[11] A. Kaya and E. Y. Y. Ksel, "A discussion on the performance of impedance matched antenna system and considerations for a better performance," Microw. & Optical Tech. Lett., vol. 50, no. 2, Feb. 2008.
[12] M. Arrawatia, M. S. Baghini, and G. Kumar, "Differential microstrip antenna for RF energy harvesting," IEEE Trans. Antennas Propag., vol. 63, no. 4, pp. 1581–1588, Apr. 2015.
[13] C. Ding, K.-M. Luk, "Low-profile magneto-electric dipole antenna," IEEE Antennas Wireless Propag. Lett., vol. 15, pp. 1642–1644, 2016.
[14] K. M. Luk, C. L. Mak, Y. L. Chow, and K. F. Lee, "Broadband microstrip patch antenna," Electron Lett., vol. 34, no. 15, pp. 1442–1443, Jul. 1998.
[15] H. Wong, K. K. So, and X. Gao, "Bandwidth enhancement of a monopolar patch antenna with V-shaped slot for car-to-car and WLAN communications," IEEE Trans. Veh. Technol., vol. 65, no. 3, pp. 1130–1136, Mar. 2016.
[16] N.-W. Liu, L. Zhu, W.-W. Choi, and X. Zhang, "A low-profile aperture coupled microstrip antenna with enhanced bandwidth under dual resonance," IEEE Trans. Antennas Propag., vol. 65, no. 3, pp. 1055–1062, Mar. 2017.
[17] C. Caloz, T. Itoh, *Electromagnetic Metamaterials: Transmission Line Theory and Microwave Applications: The Engineering Approach*, Wiley 2006.
[18] J. Xi, H. Zhu, "UHF RFID impedance matching: T-match dipole tag design on the highway," IEEE International Conference on RFID, 2015, pp. 86-93.
[19] Y. Han and D. J. Perreault, "Analysis and design of high efficiency matching networks," IEEE Transactions on Power Electronics, vol. 21, no. 5, pp. 1484-1491, Sept. 2006. DOI: 10.1109/TPEL.2006.882083.
[20] Pieter L. D. Abrie, *The Design of Impedance-Matching Networks for Radio-Frequency and Microwave Amplifiers*, Artech House, 1985.
[21] I. J. Bahl and P. Bhartia, *Microstrip Antennas*, Artech House, Dedham, MA, 1980.
[22] J. S. Roy and B. Jecko, "Simplified design for a circular microstrip patch antenna," Microwave and Optical Technology Letters, vol. 6, no. 3, 1993, pp. 201-205.
[23] Peter A. Rizzi, *Microwave Engineering – Passive Circuits*, Prentice-Hall, 1988.
[24]https://my.ece.utah.edu/~dschurig/7/ECE_5350_and_6350_Fall_2014/Assignment_1.html
[25] N.-W. Liu, L. Zhu, W.-W. Choi, and X. Zhang, "A low-profile differential-fed patch antenna with bandwidth enhancement and sidelobe reduction under operation of TM10 and TM12 modes," IEEE Trans. on Antennas & Propag., vol. 66, no. 9, Sept. 2018, pp. 4854-4859.
[26] N.-W. Liu, L. Zhu, Z.-X. Liu, and Y. Liu, "Dual-band single-layer microstrip patch antenna with enhanced bandwidth and beamwidth based on

reshaped multiresonant modes," IEEE Trans. on Antennas and Propag., vol. 67, no. 11, Nov. 2019, pp. 7127-7132.
[27] G. Muntoni, G. Montisci, G. A. Casula, F. P. Chietera, A. Michel, R. Colella, L. Catarinucci, and G. Mazzarella, "A curved 3-D printed microstrip patch antenna layout for bandwidth enhancement and size reduction," IEEE Antenna & Wireless Propag. Lett., vol. 19, no. 7, July 2020, pp. 1118-1122.
[28] J.-Y. Lee, J. Choi, J.-H. Jang, and W. Hong, "Performance enhancement in compact inverted-L antenna by using 1-D EBG ground structures and beam directors," IEEE Access, vol. 7, 2019, pp. 93264-93274.